Astron. Astrophys. 357, 1170–1180 (2000)

ASTRONOMY AND ASTROPHYSICS

Genetic eclipse mapping and the advantage of Black Sheep

A. Bobinger

Universitäts-Sternwarte, Scheinerstrasse 1, 81679 München, Germany (Andreas.Bobinger@kratzer-automation.de)

Received 8 January 2000 / Accepted 21 March 2000

Abstract. A new genetic eclipse mapping method GEM is presented. A genetic algorithm was used to reconstruct accretion disks with the Double Dataset eclipse mapping method. With the introduction of "Black Sheep" into the evolution, an increase of the speed of evolution by a factor of ten was reached. By applying the new algorithm to test data and to observational data the robustness and reliability of this new tool could be confirmed. Despite the high amount of computing time, the fitness of GEM, to be used as a reconstruction tool in the eclipse mapping algorithm, compares advantageously with the traditionally used maximum entropy package MEMSYS. The reconstructions are of high clarity and, less influenced by faulty data, not user–biased and do not require the use of an user–supplied default image. Applying this new algorithm to a dataset of the cataclysmic variable IP Peg a rough fingerprint of a spiral arm is found in the position coordinate representation of the quiescent accretion disk. This phenomenon is discussed and compared with previous works.

Key words: methods: numerical – stars: novae, cataclysmic variables – accretion, accretion disks – stars: individual: IP Peg

1. Introduction

When C.R. Darwin went aboard the MS Beagle, this was the starting point of one of the most exciting changes of mankind's perception of the world and its creation by introducing the principle of *natural selection* (Darwin 1859).

This principle is easy to code and represents the central part of all optimization-programs called *evolutionary algorithms*. The *genetic algorithms* (hereafter GAs) are a subset of these (Baeck 1996). GAs are not common in astrophysics and other sciences, despite their robustness and easy application. GAs can be applied to every optimization problem, linear or not.

In this paper a genetic algorithm to solve an inverse problem is presented. I used the slightly modified and problem adapted GA PIKAIA, created by Charbonneau (1995) as a basic tool for my *genetic eclipse mapping algorithm* GEM. This algorithm is applied instead of the maximum entropy optimizer MEMSYS (Skilling & Bryan 1984) to perform the eclipse mapping (see Horne 1985, for a description of the eclipse mapping algorithm). In Sect. 2 a short description of the genetic algorithms, eclipse mapping and Doppler tomography is given. The GEM algorithm is discussed in Sect. 3 and methods of acceleration of evolution are presented in Sect. 4. The application of GEM to test data as well as to observations is outlined in Sects. 5 and 6. A discussion and an outlook in Sect. 7 complete the paper.

2. Methods and improvements

2.1. Genetic algorithms

Genetic algorithms are not a new invention. First papers were published, describing the application of GAs in astrophysics (Hakala 1995; Charbonneau 1995; Charbonneau & Knapp 1996). Especially the article of Charbonneau (1995) is recommended for a good introduction into GAs and various examples of applications (see also Holland 1962 and Davis 1991). In recent years GAs were applied to problems in helioseismology (Charbonneau et al. 1998), spectral decomposition (McIntosh et al. 1998) and coronal modelling (Gibson & Charbonneau 1998).

GAs mimic life in the computer. First a problem has to be parameterized. This parameter set can now be regarded as an individual. Then many individuals play the game of life, evolving closer and closer towards the optimum solution for the problem. The general principles of GAs, like selection of parents, crossover, mutation and the en– and decoding of individuals are very well described by Charbonneau (1995) and Charbonneau & Knapp (1996) and the reader is recommended to read the appropriate sections in these articles.

The advantage of a genetic algorithm is its ability to explore the total parameter space with high efficiency. But contrary to Monte Carlo methods, the information of a good random result is kept in the population in genetic form and passed on to the next generation through heredity. Because of the effective exploration of the parameter space, the global optimum is found with high probability and the risk to end up in side extrema is very low compared with "classical" optimizers (Charbonneau 1995). Although genetic algorithms are less efficient than classical local methods, such as for example conjuate gradients, the result does not depend on the starting points and is not user-biased (McIntosh et al. 1998).

2.2. Eclipse mapping and Doppler tomography

Cataclysmic variable stars (CVs) are close binary systems, containing a late main-sequence star and a white dwarf primary star. Material is transferred from the Roche-lobe filling secondary star towards the primary star by means of a gas stream. Due to conservation of angular momentum an accretion disk is formed, where the action of viscosity allows the material to slowly spiral inward towards the primary star. A hot spot is formed on the disk at the stream impact region. Most of these binary systems undergo outburst states which vary in duration and brightness. Dwarf novae are a subgroup of CVs showing quasi-periodic outbursts, at intervals of tens to hundreds of days, during which they brighten by several magnitudes.

Two different methods have been developed to investigate CVs, namely eclipse mapping and Doppler tomography. The eclipse mapping method allows to get a spatial reconstruction of the intensity distribution of accretion disks from light curves (Horne 1985, 1991,1993,1995; Horne & Cook 1985; Horne & Marsh 1986; Baptista & Steiner 1993; Rutten et al. 1992a,b; Rutten & Dhillon 1994; Bobinger et al. 1997,1999).

Doppler tomography (Marsh 1988; Marsh & Horne 1988; Horne 1991) reconstructs the intensity distribution of the accretion disk in velocity coordinates. Doppler maps are computed from trailed spectra and are able to resolve and separate the intensity distribution of the individual components in a semi–detached binary system, like secondary, hot spot and disk in velocity coordinates. Both methods are now established as standard applications to investigate the accretion dynamics in disks of cataclysmic variables. The classical eclipse mapping uses the maximum entropy fitting package MEMSYS (Skilling 1981; Skilling & Bryan 1984) to compute a maximum entropy reconstruction of an accretion disk, using an one dimensional light curve as input dataset. In a cataclysmic variable with a sufficiently high inclination, the accretion disk and all related light sources like the hot spot, the white dwarf or any emitting structure in the disk undergo a periodical eclipse by the secondary star, creating an unambiguous feature in the light curve. The eclipse mapping method reconstructs the intensity distribution of the accretion disk on a two-dimensional grid, in order to fit the observed data within a maximum allowed χ^2 deviation, called CAIM[1]. MEMSYS is thereby varying the intensity of the pixel grid until the χ^2 of the model reaches CAIM. Then the pixel values are varied to maximize a defined image entropy, holding the constrained $\chi^2 =$ CAIM. The image entropy is maximized with respect to a default image. The influence of the default image to the reconstruction is discussed in Bobinger et al. (1999). Contrary to the classical eclipse mapping, I used a polar grid and a concave disk with an outward facing rim. This rim consists of three pixel rows and allows to reconstruct anisotropic light sources, like the hot spot, which produces phase dependent intensity variations in the light curve like the hump.

The method was also enhanced to the so-called Double Dataset eclipse mapping (Bobinger et al. 1999). In addition to the light curve, simultaneously recorded trailed spectra are used as a second dataset. By assuming a Keplerian velocity field for the disk, it is possible to reconstruct accretion disks nearly free of artifacts. For details see Bobinger et al. (1997), Rutten (1998) and Bobinger et al. (1999).

3. Genetic eclipse mapping

The difference between the Double Dataset eclipse mapping (Bobinger et al., 1999) and the genetic eclipse mapping GEM is the use of the slightly modified genetic algorithm PIKAIA[2] (Charbonneau 1995) instead of MEMSYS (Skilling & Bryan 1984). The accretion disk population is encoded as follows: Each disk consists of 612 surface elements[3]. To all of these elements an intensity value is assigned. All the intensity values are normalized to the interval [0;1] and encoded to the sixth digit. For example the value 0.123456 would become the digit–string $(1, 2, 3, 4, 5, 6)$. So every disk could be regarded as a single cell individual with 612 chromosomes and six genes per chromosome, encoded in base 10. The crossover and mutation operators where therefore applied for every individual to all of its 612 chromosomes separately. The standard PIKAIA would use one gen-sequence, i.e. one chromosome of length $612 \times 6 = 3672$ and applie the crossover and mutation operators therefore for each individual only one time. Trial runs turned out a higher speed for using the multi-chromosome crossover and mutation, than for the standard single-point crossover and mutation (the dependence of performance-speed from the size of the problem remains to be investigated. For smaller problems, the single-point crossover and mutation might be better (Charbonneau 1999, priv. comm.).

The fitness of each individual is calculated by the following formula, called Fitness–Function (hereafter FF):

$$F_i = \frac{1}{\chi_i^2 + \lambda \times G_i}, \tag{1}$$

whereby F_i is the fitness value for individual i. The χ_i^2 measures the deviation between the data produced by the individual i and the data to fit. G_i is a value that denotes the *granulation* of the individual i. A sum over all geometrical means of all neighbors of all pixels to calculate the G_i value is used. This value gets lower the smoother the disk is, and plays a similar role as the entropy in MEMSYS. But contrary to MEMSYS this G_i value is independent of a default comparison image! The influence of the default image to the reconstruction performed with MEMSYS is discussed in Bobinger et al. (1999). By construction the G_i value is lower for one pixel with a certain intensity than for two pixels with half the intensity. The effect is that structures are concentrated as much as possible, but the χ^2 constraint is respected. But here other methods are possible, including a default dependent entropy like in MEMSYS.

[1] In this paper the reduced χ^2 value is used, i.e the χ^2 divided by N.

[2] PIKAIA was run with its default settings. See Charbonneau & Knapp (1996) for details for example concerning the variation of the mutation rate.

[3] 34 azimuthal sections, 15 radial sections plus 5 sections for the rim, also divided into 34 azimuthal sections.

Table 1. Representative journal of catastrophes: $\chi^2_{\rm final}$ is the χ^2 value at the end of the run. $N_{\rm cat}$ denotes the number of catastrophes applied and $\Delta_{\rm gen}$ the number of generations between the catastrophes. $N_{\rm gen}$ and N_{pop} are the total number of generations and the number of individuals in the population respectively. $N_{\rm BS}$ is the number of "Black sheep". All catastrophes were run with PIKAIA's default settings, but with multi-chromosome crossover and mutation (details in the text).

Catastrophes:	No Catastrophe	Part. Random Reinitialisation	Increase of Genetic Variation	"Black Sheep"
$\chi^2_{\rm final}$	644.5	559.6	541.0	3.6
$N_{\rm cat}$	–	3	3	–
$\Delta_{\rm gen}$	–	500	500	–
$N_{\rm gen}$	2000	2000	2000	2000
$N_{\rm pop}$	128	128	128	128
Comments	–	60% Replacement	20% Variation	$N_{\rm BS} = 28$, 10% Variation

The λ parameter is calculated in each generation anew (like in MEMSYS in each iteration step (Skilling & Bryan 1984). Its aim is to give about the same level of influence to both attributes, the χ^2_i (ability of an individual to fit the data) and the G_i (less and concentrated structures on the disk–individual surface). An example will illustrate the idea behind it: Imagine nature having the job to create a fast-swimming thing. It might be a better way to create an animal that has both attributes at the same time during the evolutionary process, because something that is fast, is not necessarily a good swimmer (swallow, cheetah) and something that is swimming well might not be fast (coconut, jellyfish)! In the FF the normal phenotype parameters are rescaled to their "true" values and the corresponding light curve and trailed spectra for each individual are calculated. From this the global data–χ^2_i and the surface intensity granulation value G_i for each individual are calculated, from which the fitness F_i for the individual is determined. When the χ^2_i value of an individual is lower than or equal to the CAIM target value, the χ^2_i value was set to CAIM, leaving the G_i value as only operating fitness criterion. So when the χ^2 target CAIM was reached, only the granulation was improved during the following generations (see also the captions of Figs. 3 and 4). The question when to terminate the evolution is discussed in Sect. 7.

4. Catastrophes and other Black Sheep

To make life more realistic to the accretion disk population, catastrophes and "Black Sheep" were introduced.

In earth's history several serious catastrophes happened. A big meteor impact near the coast of America is supposed to have caused the extinction of the dinosaurs. What was a catastrophe for the dinosaurs was an opportunity for the mammals. It is also supposed, that the magnetic field of our earth has reversed polarity several times. The last time this happened, coincided with the erectness of some primates. All these catastrophes are discrete catastrophes which lead to a jump in the evolutionary process. *Black Sheep* are a special case of catastrophes, i.e. individuals not completely in conformity with the common trends and customs. They are acting in each generation like a permanent catastrophe.

The above mentioned catastrophes are a good way to bring additional variation into the population beside the natural mutation. They inspired the following "software-catastrohes":

- **Partial Random Reinitialisation Catastrophe (Meteor)**
  A big amount of the population (for example 60%) is randomly replaced by a new random population (but in contrast to reality, elitism[4] still works in the algorithm). This catastrophe is nothing more than a partial random re–initialisation of the population.
- **Increase of Genetic Variation Catastrophe (Magnetic Field)**
  All genetic information (i.e. every surface element) in the total population is varied by a random generator within certain limits (for example $\pm 20\%$). The global shape of the individuals is preserved, but they get locally noisy.
- **"Black Sheep" Catastrophe**
  Black Sheep are created in every generation anew and are therefore a permanent catastrophe. They are randomly distorted copies (for example 10%) of the fittest individual. So they are similar to the Magnetic Field catastrophe but apply only to the nearest neighborhood of the fittest individual (mutate-best-replace-worst). They can be regarded as a sort of *"fitness gradient patrol"* around the current optimum (i.e. around the fittest individual).

Some trial runs were made to test the influence of catastrophes to the speed of evolution. For the test an artificial dataset, described in Sect. 5, was used. Because of the high amount of computational time, the trial runs were stopped after 2000 generations. In every case a relatively small population of 128 individuals was used. Each discrete catastrophe was applied three times per run, i.e. each time after 500 generations. The Meteor impact was simulated by randomly replacing 60% of the population. The reversing of the Magnetic Field was simulated by varying the genes of all individuals in their phenotype representation randomly within 20%. Black Sheep, as a permanent catastrophe, were created by replacing the 28 worst individuals with images of the fittest individual, which was varied in its genes randomly by 10% in every generation.

Table 1 shows a representative listing of the catastrophes and their influence. In the first line the reached χ^2 value is presented. All catastrophes had a good influence on the evolution which can be seen from the lower χ^2 values compared with the

[4] Elitism means, that the current fittest individual is preserved and enters the next generation unchanged.

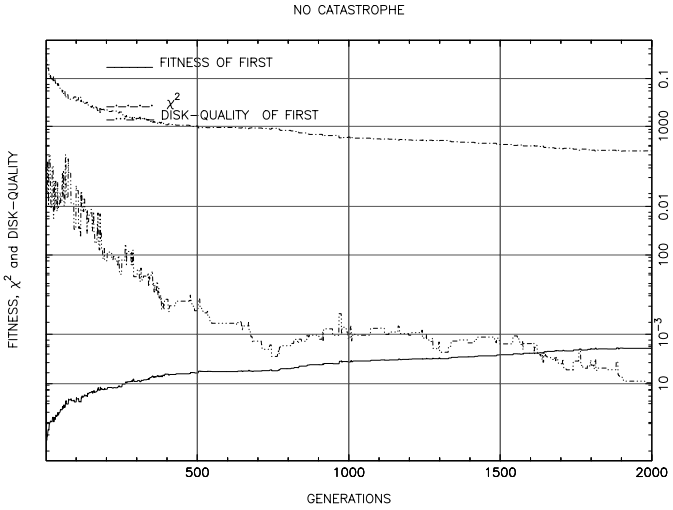

Fig. 1. Representative trace of the evolution when no catastrophe has occurred. Fitness (———), granulation G (-...-...-) and χ^2 (-.-.-.-) of the fittest individual in the population are plotted over the generation number. The abscissas are scaled logarithmically. The final values of χ^2, granulation G and Fitness of this "first" individual are listed in Table 1. χ^2 and granulation G are basically decreasing with roughly constant logarithmic "evolution–speed".

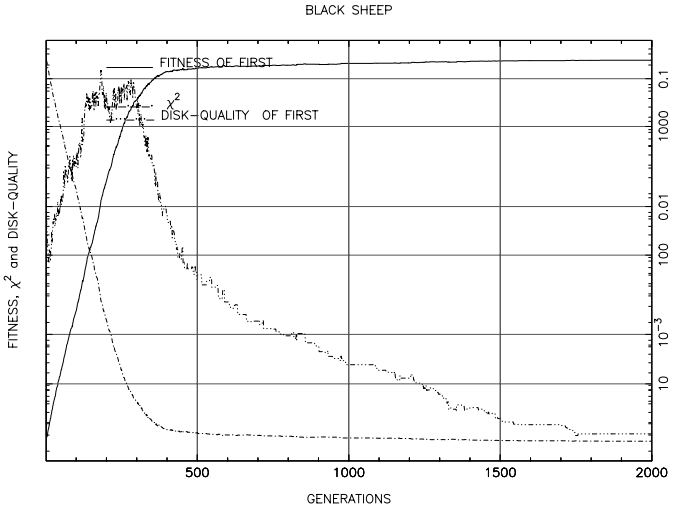

Fig. 2. Representative trace of the evolution when Black Sheep as permanent catastrophe are applied. Fitness (———), granulation G (-...-...-) and χ^2 (-.-.-.-) of the fittest individual in the population are plotted over the generation number. The abscissas are scaled logarithmically. The final values of χ^2, granulation G and Fitness of this "first" individual are listed in Table 1. Note that the granulation is rising during the first 350 generations, while the χ^2 value is dropping with a highly increased speed, compared with the "no–catastrophe" case, presented in Fig. 1.

final χ^2 value when no catastrophe occurs (first column). It is obvious that the Black Sheep seem to be the "best" catastrophe. And indeed, the speed of evolution is accelerated by about a factor of 10! To reach χ^2 = 1 with no catastrophes about 100000 generations were needed, whereby only 10000 generations were necessary by applying Black Sheep.

The Figs. 1 and 2 present the evolution of fitness (———), G (-...-...-) and χ^2 (-.-.-.-) of the fittest individual in the population during 2000 generations. Both plots have the same scales, whereby the abscissas are logarithmic. The final χ^2 values are listed in Table 1.

5. Application to test data

In order to test the GEM algorithm, a model accretion disk map was created. This map has increasing intensity towards the center and a hot spot at the rim near the impact region of the gas stream. To test the feasibility of the reconstruction algorithm to non-axisymmetric light sources, a second spot was added onto the disk. From this artificial disk a light curve was calculated and Gaussian noise was added to simulate real data. This light curve was then used as input data to the GEM algorithm to reconstruct the original map. From this map a trailed spectrum was also calculated, by assuming a Keplerian velocity field, to transform the map from position coordinate representation into trailed spectra. Also Gaussian noise was added to the spectrum to simulate real data. Doppler tomography now allows to calculate the intensity distribution of the original map in velocity-coordinates by using this trailed spectra as input data. Fig. 3 shows in four sub-panels the artificially created map (B), the derived light curve (A), the trailed spectra (C) derived from the map (b) and finally the Doppler-map (D) calculated from the trailed spectra, assuming a Keplerian velocity field for the disk. The arrows between the panels should clarify the data-flow. Fig. 4 shows the GEM reconstruction of the original map, using the light curve (Fig. 3A) and the trailed spectra, derived from the map in Fig. 3B, under the assumption of a Keplerian velocity field, as a double dataset (see also Bobinger et al. 1999). In Fig. 4 the fittest individual of the population is plotted. The quality of the reconstruction is good and comparable to the reconstruction quality reached by using a maximum entropy algorithm as an optimizer (see Fig. 5 of Bobinger et al. 1999). The slight "granulation" in the map (Fig. 4B) reflects the genetic variation of the population, which makes it fit to survive and allows the population to evolve away from side–extrema.

6. Application to observational data

6.1. The dataset

During an observing campaign in August 06–09 1994 simultaneous spectroscopy at the 3.5m and spectrophotometry at the 2.2m telescopes at the German-Spanish Astronomical Center, Calar Alto, Spain, were performed, to obtain data from the cataclysmic variable IP Peg during quiescence. From the trailed spectroscopic dataset the H_γ, H_β and H_α Balmerlines were extracted. The spectrophotometric data were recorded with the MEKASPEK device of the Universitäts-Sternwarte München (Mantel & Barwig 1993; Mantel et al. 1993,) and enabled us to extract photometric light curves of the Balmer lines H_γ, H_β and H_α. Data acquisition and the reduction methods used are described and explained in detail in Wolf et al. (1998), Šimić et al. (1998) and Bobinger et al. (1999). For a discussion about

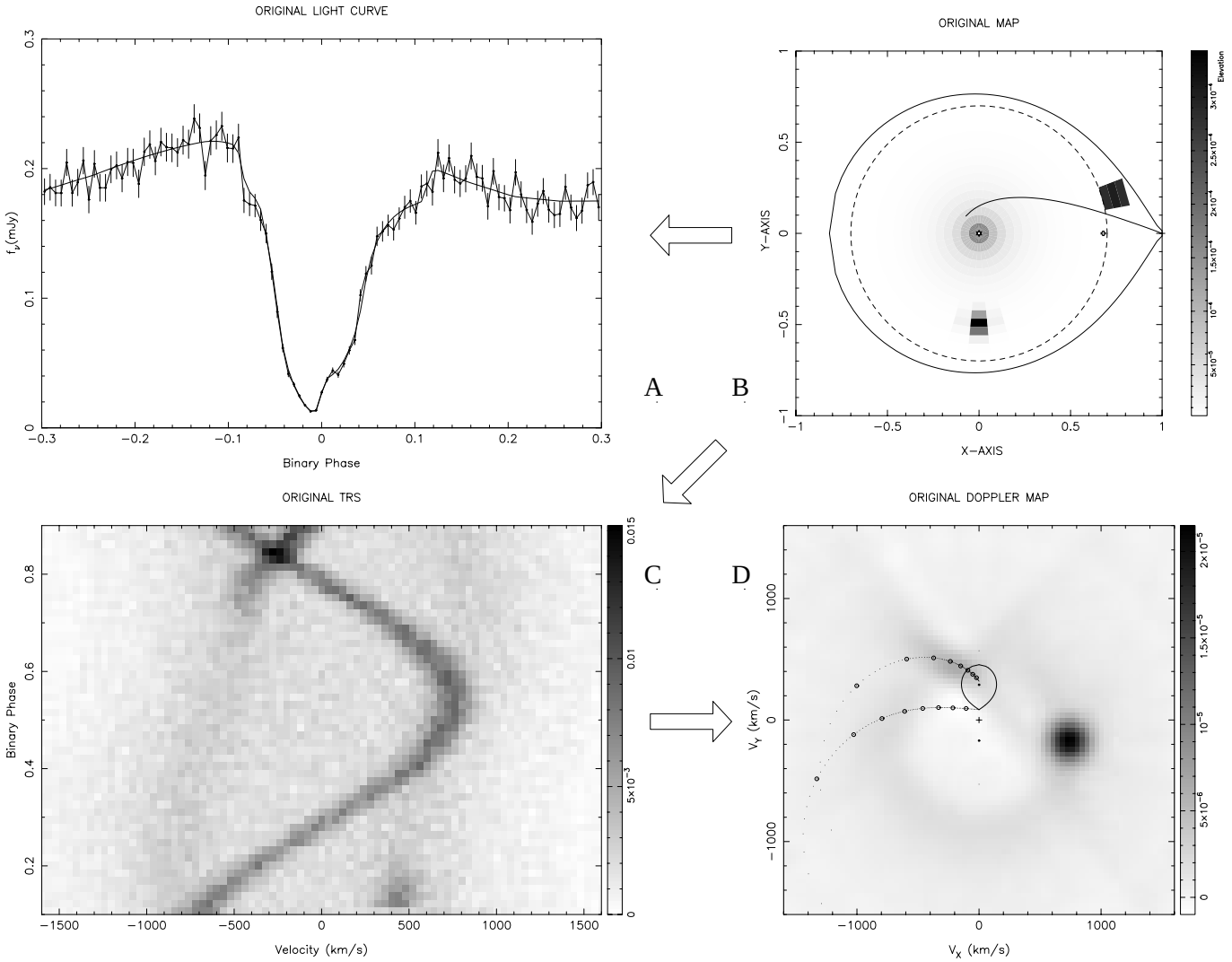

Fig. 3. Original test map: (A) light curve between phase -0.2 and +0.2. in arbitrary units, derived from the map displayed in (B). (B) Intensity distribution of the test map in position-coordinate representation. The dashed circle represents the outer disk radius. Pixels outside the dashed circle belong to the rim and are folded upward for plotting reasons. Also the Roche lobe and the gas stream trajectory are plotted. The unit is the distance between the white dwarf and the inner Lagrangian point L_1. (C) Trailed spectra derived from the map in (B), assuming a Keplerian velocity field. (D) Doppler map, reconstructed from the trailed spectra shown in (C) with a Fourier filtered back projection algorithm. A schematic overlay marks the Roche lobe of the secondary as well as the ballistic trajectory which originates from the L_1 point. Additionally plotted is a second trajectory which represents the velocity of the disk along the path of the gas stream (upper trajectory).

the secondary see also Wolf et al. (1998) and Bobinger et al. (1999). These articles also contain a detailed description and discussion of the geometry used for reconstruction.

6.2. The results

The original trailed spectra and the H_γ, H_β and H_α emission line light curves as input dataset were used, to reconstruct the accretion disk of IP Peg in these emission lines. Panels A show the smoothed (boxcar filtered) Balmer line light curves derived from the MEKASPEK dataset and the fit (solid line) to the data. In panels B the fittest individuals of the GEM reconstructions are plotted, panels C present the trailed spectra derived from the fittest individuals shown in panels B. In panels D the Doppler maps, derived from the trailed spectra in panels C, are presented. For all GEM reconstructions between 50000 and 60000 generations were necessary. The χ^2 target CAIM was reached in all cases within the first 25000 generations. The remaining generations were used to improve the smoothness of the population (see Sect. 7 for a discussion about the termination of the evolutionary process).

7. Discussion and outlook

The GEM reconstructions in position coordinates (Figs. 5B, 6B, 7B) show more structure as their MEMSYS counterparts in the paper of Bobinger et al. (1999). The MEMSYS reconstructions are smoother and look locally different especially in H_γ and H_α

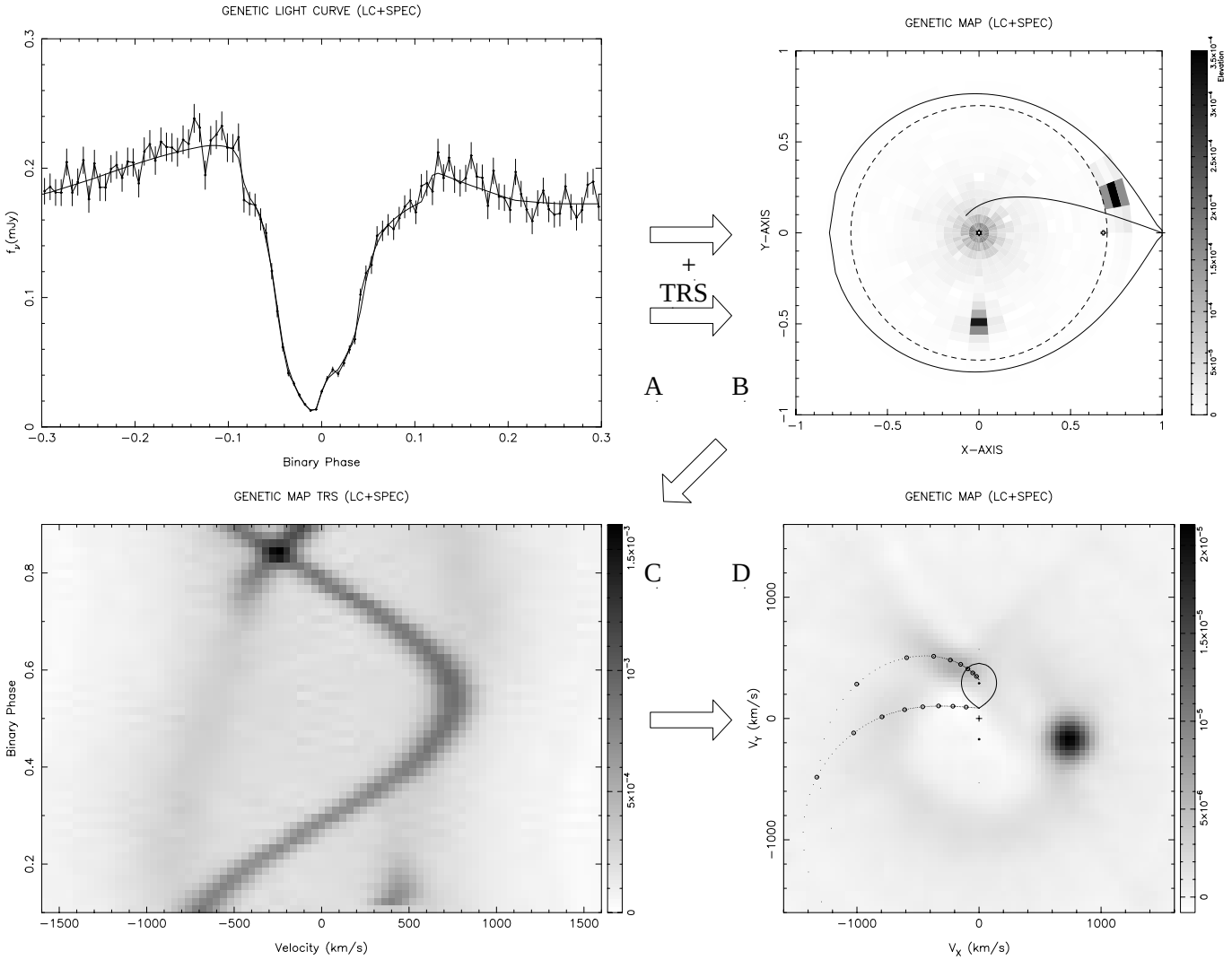

Fig. 4. Genetic Double Dataset Reconstruction of the original map, shown in Fig. 3B, using the light curve and the trailed spectra shown in Fig. 3A,C as the input dataset. (A) in this plot shows the input data and the fit to the light curve (solid line). (B)shows the reconstruction in space-coordinate representation. (C) presents the trailed spectra, derived from the map in (B) under the assumption of a Keplerian velocity field. (D) visualizes the corresponding Doppler-map in velocity-coordinates. The genetic reconstruction was stopped after 40000 generations. $\chi^2 = 1$ was reached about during the first 10000 generations. During the remaining 30000 generations, only the attribute "granulation" was optimized.

(The reader is encouraged to compare the results with the numerical simulations of Makita et al. 1998). The Doppler maps, derived from the reconstructions, are a valuable criterion to judge the quality of the reconstruction. They only have to be compared with the original Doppler maps derived directly from the observed trailed spectra.

In order to visualize the different reconstruction qualities, all Doppler mapping results are plotted in Fig. 8. The Doppler maps derived from the original trailed spectra (taken from Wolf et al. 1998) are plotted in the top row (H_γ, H_β and H_α from left to right). In the second row from top, the Doppler maps derived from the Double Dataset GEM reconstructions are shown (this paper). The third row from top shows the Doppler maps derived from the Double Dataset MEMSYS reconstruction (taken from Bobinger et al. 1999). In the bottom row the Single Dataset MEMSYS reconstruction (from Wolf et al. 1998) are presented.

Taking the top row as a benchmark for quality, the Double–Dataset reconstructions are superior than the reconstruction where only the light curve was used as input dataset. But the MEMSYS and the GEM reconstructions show internal differences, depending on the optimizer used. The first is the different χ^2 handling. MEMSYS is a gradient algorithm. It calculates not only the entropy gradient, but also a χ^2 gradient map. This χ^2 gradient map is very sensitive incorrect error estimates. The error bars in the trailed spectra were derived from photon statistics, i.e. the error is $\propto \sqrt{countrate}$. If a erroneous spectrum has a low count rate, then its corresponding error is also low. But low error means high weight for MEMSYS. The algorithm will try to make the fit closer to this wrong data points than to the correct ones. GEM has the advantage to work with a *global* χ^2 number and ignores wrong data points automatically. The second difference is the user bias of the MEMSYS results. This user bias

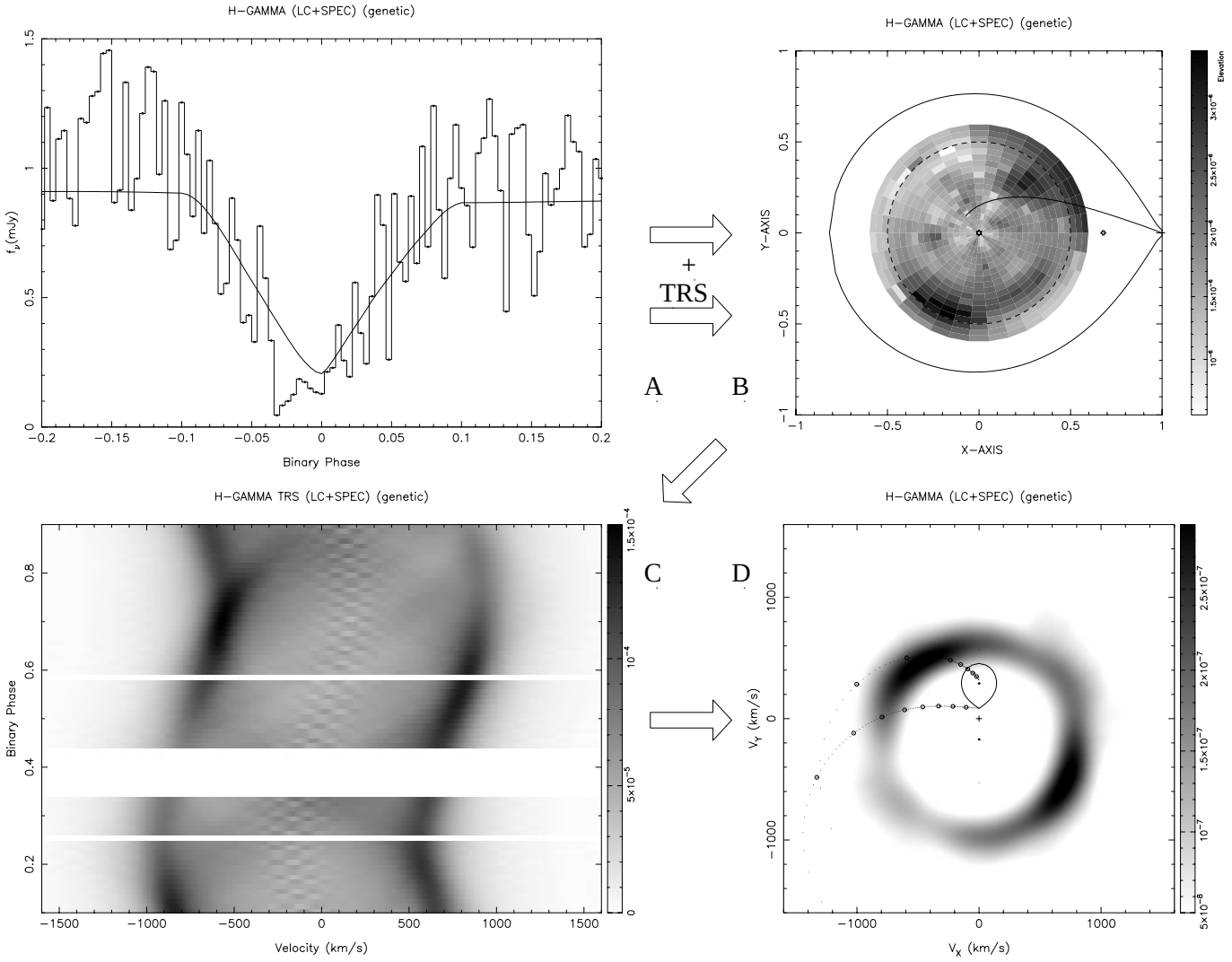

Fig. 5. Genetic Double Dataset reconstruction in H_γ, using the light curve and the trailed spectra as input dataset. The fittest individual of the population is plotted. The arrows between the panels clarify the data-flow. (A) shows the input data and the fit to the light curve (solid line). (B) shows the reconstruction in position coordinate representation. The dashed circle represents the outer disk radius. Pixels outside the dashed circle belong to the rim and are folded upward for plotting reasons. Also the Roche lobe and the gas stream trajectory are plotted. The unit is the distance between the white dwarf and the inner Lagrangian point L_1. (C)presents the trailed spectra, derived from the map in (B) under the assumption of a Keplerian velocity field. Missing phase–ranges due to data gaps are marked with white empty rows. (D) visualizes the corresponding Doppler map in velocity coordinates. A schematic overlay marks the Roche lobe of the secondary as well as the ballistic trajectory which originates from the L_1 point. Additionally plotted is a second trajectory which represents the velocity of the disk along the path of the gas stream (upper trajectory).

comes in, when the starting image has to be defined. When the starting image is too high (low) at the very beginning, the result will be also too high (low) in some regions of the reconstructed disk. Especially in this regions which have week correlations do the data, for example the outer regions of the disk. A lack of intensity in the outer regions of the disk can be compensated by an increase of intensity in the disk rim and vice versa. This user bias was not found in the GEM reconstructions, as simulations show. Because of this I take the GEM reconstructions for the more reliable ones.

One exception is the H_α reconstruction. Because the trailed spectra dataset in H_α covers only the phase range between 0.42 to 0.9 (less than 50% of the total phase), the light curve fit in Fig. 7A shows a low quality in the phase range after the eclipse. The flux level is too low there. Despite their robustness with respect to wrong data, the GA has difficulties to deal with incomplete datasets. The global χ^2 handling, being an advantage in dealing with wrong data, is now a handicap. MEMSYS reconstructs the H_α light curve very well (see Fig. 9A in Bobinger et al. 1999), because it is a gradient algorithm and respects all data points via the corresponding χ^2 gradient map. GEM has no chance to do so, because it has no information about the "local" χ^2 gradients of the data points. Therefore a dataset as complete as possible is necessary to run GEM properly.

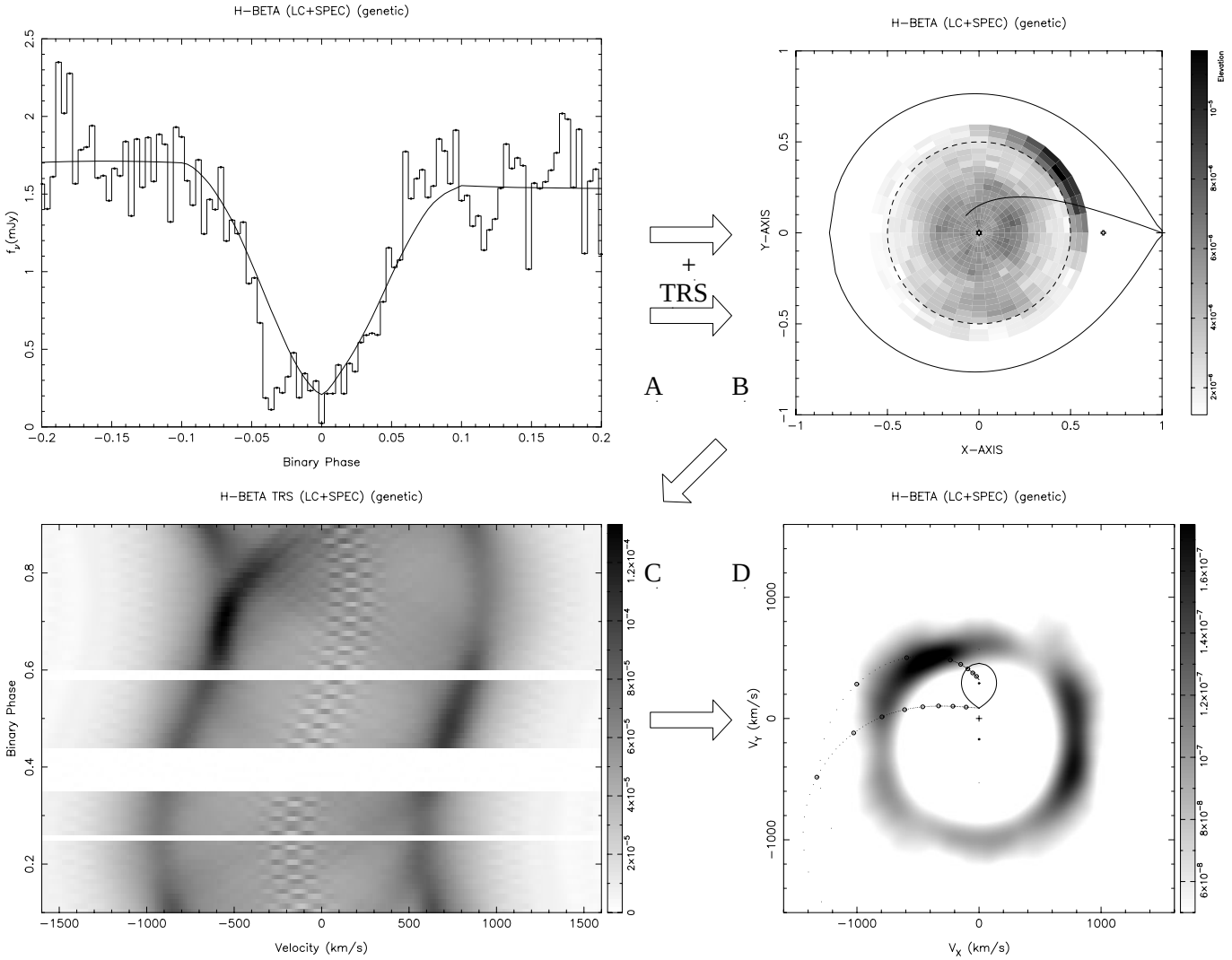

Fig. 6. Genetic Double Dataset reconstruction in H_β, using the light curve and the trailed spectra as input dataset. The fittest individual of the population is plotted. The arrows between the panels clarify the data-flow. (A-D) are described in Fig. 5.

When Steeghs et al. (1997) detected spiral structures in the accretion disk of the cataclysmic variable IP Peg, the notion about accretion disks changed. They are not describable by only one linear (radius–) dimension but need a 3-dimensional description. The feasibility and observability of spiral structures in accretion discs are discussed in Bunk et al. (1990) and in Steeghs & Stehle (1998), respectively. A discussion about the impact of spirals to the standard accretion disk model is given in Sawada et al. (1987). The origin of these spirals is not completely settled up to now, but one reason might be that they are tidally induced by the secondary star (Savonije et al. 1994). Simulations of spiral structures in IP Peg were performed by Armitage & Murray (1998) and Matsuda et al. (1998). Advanced three dimensional particle simulations of accretion discs, yielding shocks and spirals, were calculated by Yukawa et al. (1997), Makita et al. (1998) and Boffin et al. (1998) respectively. Comparing the Fig. 2 in Yukawa et al. (1997), Fig. 4 in Makita et al. (1998) and Figs. 1 and 2 in Boffin et al. (1998) with our Balmer line reconstructions (especially H_γ, Fig. 5), a moderate concordance can be seen, despite the relatively poor signal to noise ratio of the dataset used. All simulations made by the previous mentioned authors show one or two spirals in the disk which are counterclockwise winding inward. This structures are originating from the impact region of the gas stream (hot spot) and are forming an annulus–like structure in the inner regions of the disk (the spirals are wound up more narrow as they go inward). The second spiral arm, which is rotated by π and therefore originating roughly opposite to the hot spot, leads to an increased density in the "lower" part of the accretion disk, i.e about at space coordinates $(X;Y) = (0.0;-0.3)$ or at velocity coordinates $(V_X;V_Y) = (+800;0.0)\,km\,s^{-1}$. The bright spot in the reconstructions at this coordinates (see Fig. 6, Fig. 7 and especially Fig. 5) can be therefore regarded as a rough fingerprint of such a spiral arm (compare with Fig. 2 in Matsuda et al. 1998). This raises the hope, that it will be possible to reconstruct spiral structures in space coordinate representation with reliable

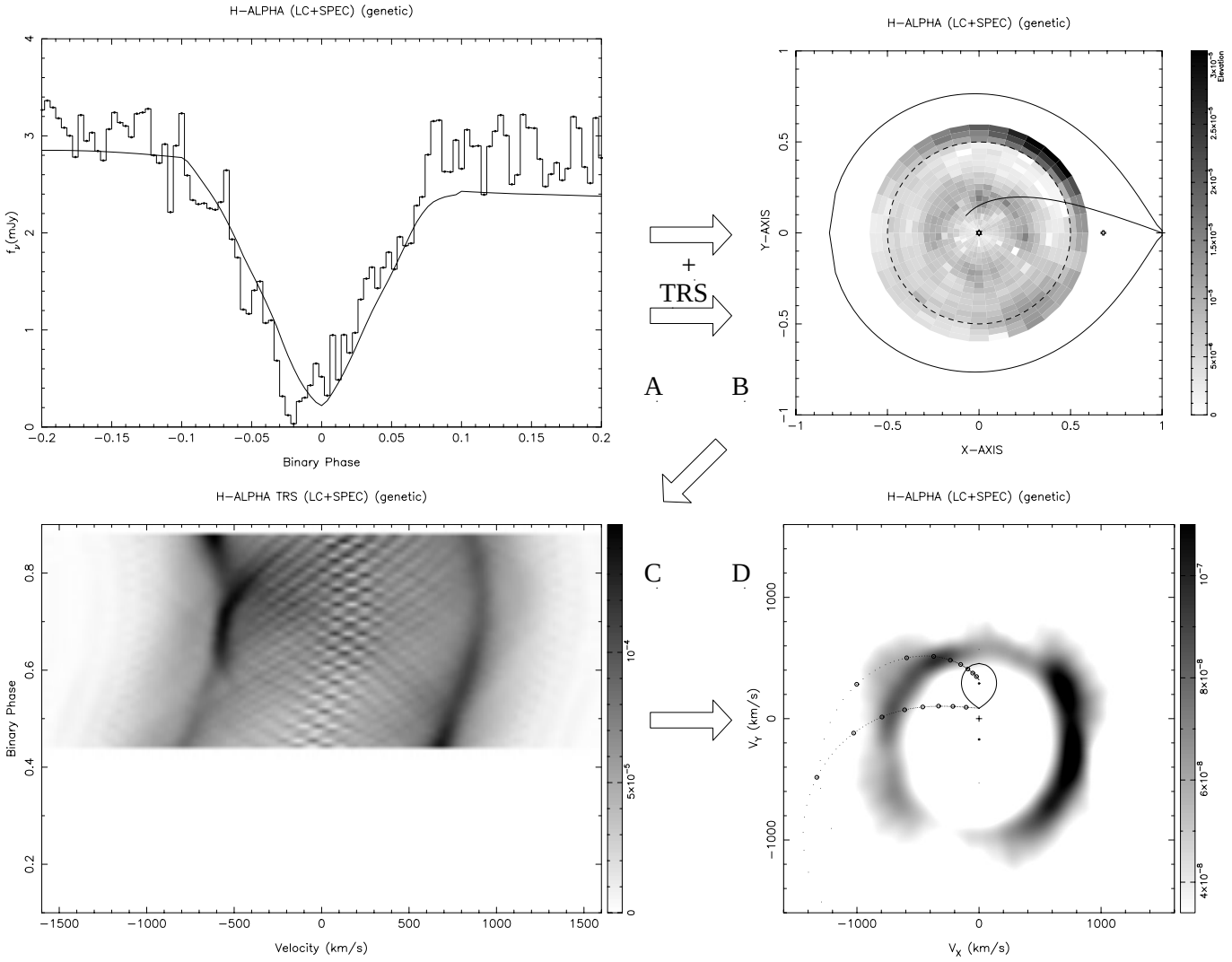

Fig. 7. Genetic Double Dataset reconstruction in H_α, using the light curve and the trailed spectra as input dataset. The fittest individual of the population is plotted. The arrows between the panels clarify the data-flow. A-D are described in Fig. 5. Note that we could obtain only 50% phase coverage in H_α.

clearity, using datasets with a better signal to noise ratio. To do this, simultaneous spectro–photometry and spectroscopy at large telescopes are necessary. The spectroscopic task would be to record trailed spectra and the spectro–photometry would provide the possibility to extract the emission lines from the underlying continuum and to get emission line light curves of the CV. Such datasets, with high enough signal to noise ratio, would allow to reconstruct the accretion disks with a high time resolution and to follow the evolution of the assumed spirals. This could answer the question as to whether the angular momentum transport in accretion disks is due to viscous processes or to spirally shaped shock fronts(see Sawada et al. 1986a,b, 1987; Spruit 1989).

Double Dataset eclipse mapping gives better reconstructions, but together with genetic algorithms a further increase of reconstruction quality is possible. The GEM algorithm turns out to be very robust and non–sensitive with respect to wrong data and error bars and is not user biased. The algorithm is easy to code, no matrix operations had to be carried out, no gradients to be calculated. The risk to end in a side–extrema is very low for a "typical" optimization problem.

But there are also some disadvantages: One problem is to decide when to stop the evolution. Any "classical" (or mathematical) optimizer can reach the top of an extremum exactly. But when the fitness function depends on different quantities, such as χ^2 and granulation, things are more complicated. For the χ^2 criterion some limit (usually CAIM = 1.0) can be defined. But it is not clear what granulation value is a good one. It is also difficult at some evolutionary stages to distinguish between granulation and structure. When the evolution is more advanced, the fitness gradient might be very low. At this evolutionary stages one has to wait a long time (despite the Black Sheep) to improve the fitness of the population. This leads to some subjectivity in the reconstruction. The user has to decide to stop or to go on. But this is *the* central difficulty in all heuristic search techniques.

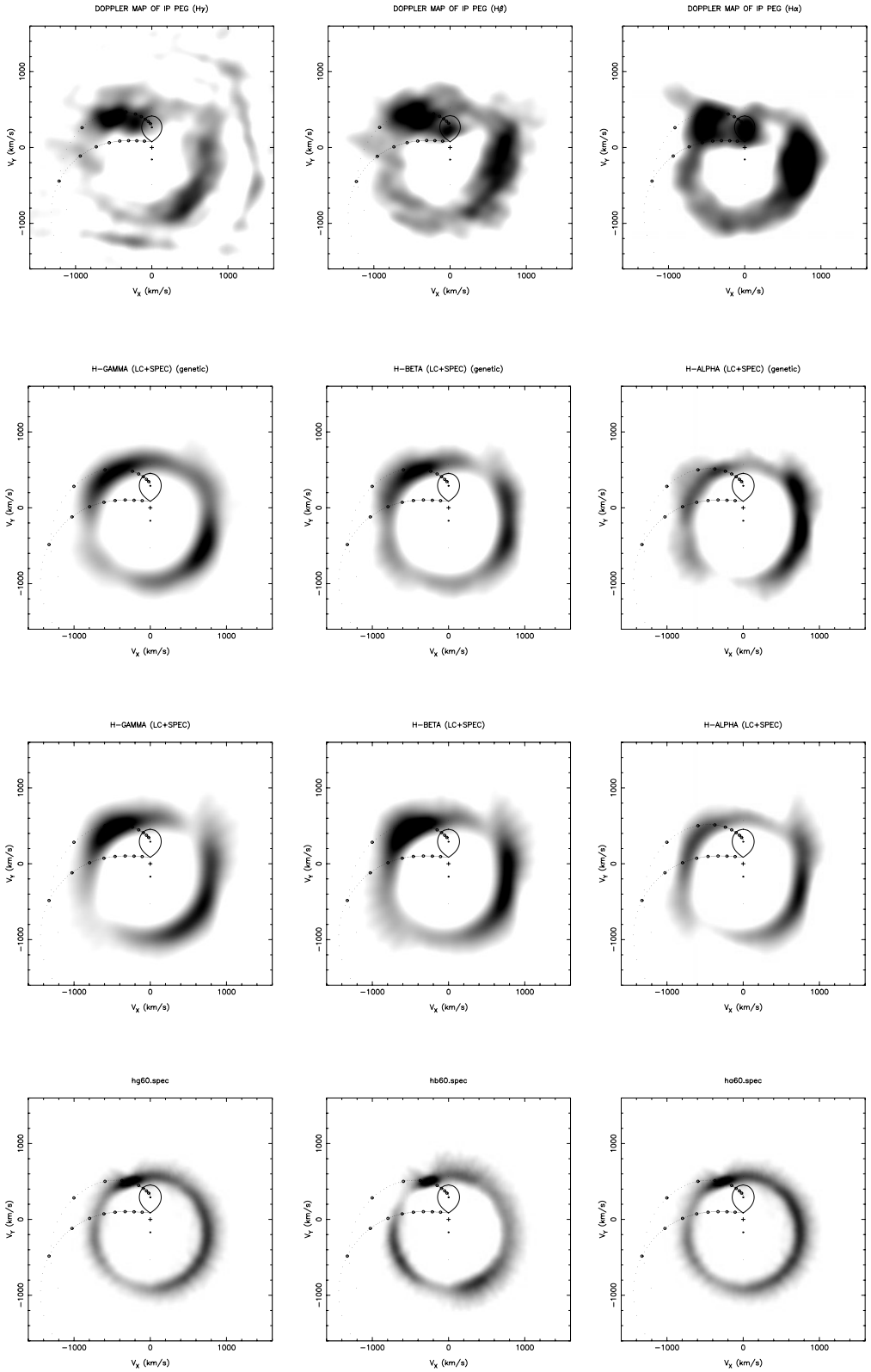

Fig. 8. Doppler maps reconstructed with a Fourier filtered back projection algorithm. (H_γ, H_β and H_α from left to right): Top row: Doppler maps from the original trailed spectra. Second row from top: Doppler maps calculated from the spectra derived from the GEM reconstructions. Third row from top: Doppler maps calculated from the spectra derived from the Double Dataset MEMSYS reconstructions. Bottom row: Doppler maps calculated from the spectra derived from the Single Dataset MEMSYS reconstructions. A schematic overlay marks the Roche-lobe of the secondary as well as the ballistic trajectory which originates from theL_1 point. Additionally plotted is a second trajectory which represents the velocity of the disk along the path of the gas stream (upper trajectory).

Another point is the high amount of computational time. With MEMSYS the reconstructions were made in about three hours CPU time, GEM needed almost three weeks (on a DEC 3000 175MHz Workstation). But highly parallelized computers could change things in the future. A computer with, for example 500 processors and running a (parallelized) GEM algorithm would be even faster than MEMSYS today, when each processor calculates one individual of the population (even without Black Sheep).

To speed up evolution, Black Sheep seem to be a good method. Black Sheep are surrounding the fittest individual like an "exploring cloud", searching for better solutions in the nearest neighborhood of the fittest individual. They act like a rather strange gradient optimizer[5].

A possible extension of the algorithm will be the Triple Dataset eclipse mapping. Using the Doppler maps derived from the original trailed spectra, it should be possible to reconstruct also the velocity fields (azimuthal & radial) by adding two "velocity cells". Comparing the top row and the second row of Doppler maps in Fig. 8 it turns out, that the region around the hot spot (velocity coordinates $(V_X; V_Y) = (-600; +400)\, km\, s^{-1}$) is not properly reconstructed. The reason is that the assumed velocity field, used to transform the map in space coordinate representation into trailed spectra, is not valid in the hot spot region. There the velocities of the outer disk and the in-falling gas stream are mixed. This region also can be expected to be very turbulent (for a interesting discussion about the hot spot region and their appearance in Doppler maps see Spruit & Rutten 1998). By introducing the velocity cells into the evolutionary process and by adding the original Doppler maps to the light curve and trailed spectra as third dataset, this region should be reconstructed well, yielding the corresponding velocity field. Such a project needs new datasets with a good signal to noise ratio, recorded at large telescopes. Complete datasets, covering a total period, could make "*velocity mapping*" possible.

Acknowledgements. The author would like to say Thank You to all the helpful CV-people in our institute and at MPA and MPE Garching, for many fruitful discussions. To H. Barwig for being the best chief one can imagine and to K.H. Mantel for helpful advice and assistance during the time of my thesis. A. Bobinger is especially thankful to H. Fiedler, D. Šimić and S. Wolf for inciting him to do this work and for their reliance into the "impossible". Also many thanks to K. Horne, for the basic eclipse mapping programs and encouraging me to go new ways.

References

Armitage P.J., Murray J.R., 1998, MNRAS 297, L81
Baeck T., 1996, Evolutionary Algorithms in Theory and Practice. Oxford UP, Chap. 2
Baptista R., Steiner J.E., 1993, A&A 277, 331
Bobinger A., Horne K., Mantel K.H., Wolf S., 1997, A&A 327, 1023
Bobinger A., Barwig H., Fiedler H., et al., 1999, submitted to A&A
Boffin H.M.J., Haraguchi K., Matsuda T., 1999, In: Mineshige S., Wheeler J.C. (eds.) 25 Years of the Disk–Instability Model. Universal Academy Press (astro–ph/9812010)
Bunk W., Livio M., Verbunt F., 1990, A&A 232, 371
Charbonneau P., 1995, ApJS 101, 309
Charbonneau P., Knapp B., 1996, A Users Guide to PIKAIA 1.0: NCAR Technical Note 418+1A
Charbonneau P., Tomczyk S., Schou J., Thompson M.J., 1998, ApJ 496, 1015
Darwin C.R., 1859, On the Origin of Species by Means of Natural Selection. On the Preservation of Favoured Races in the Struggle for Life. J. Murray, London
Davis L., 1991, Handbook of Genetic Algorithms, Van Nostrand Reinold
Gibson S.E., Charbonneau P., 1996, Journal of Geophysical Research 103, A7, 14511
Hakala P., 1995, A&A 296, 164
Holland J.H., 1962, J. Assoc. Comp. Mach 3, 297
Horne K., 1985, MNRAS 213, 129
Horne K., 1991, In: Shafter A.W. (ed.) Fundamental Properties of Cataclysmic Variable Stars. 12th North American Workshop on Cataclysmic Variables and Low Mass X-ray Binaries. San Diego 3–5 Jan 1991, San Diego State University Publication, p. 23
Horne K., 1993, In: Wheeler J.C. (ed.) Accretion Disks in Compact Stellar Systems. World Scientific Publishing Company
Horne K., 1995, A&A 297, 273
Horne K., Cook M.C., 1985, MNRAS 216, 307
Horne K., Marsh T.R., 1986, MNRAS 218, 761
Makita M., Miyawaki K., Matsuda T., 1998, astro–ph/9809003v2
Mantel K.H., Barwig H., 1993, NATO ASI series, C436, 329
Mantel K.H., Barwig H., Kiesewetter S., 1993, In: Butler C.J., Elliot I. (eds.) Proc. of the IAU Coll. 136: Stellar Photometry, Dublin, Cambridge University Press, p. 172
Marsh T.R., 1988, MNRAS 231, 1117
Marsh T.R., Horne K. 1988, MNRAS 235, 269
Matsuda T., Makita M., Yukawa H., Boffin H.M.J., 1998, astro–ph/9807239v2
McIntosh S.W., Diver D.A., Judge P.G., et al., 1998, A&AS 132, 145
Rutten R.G.M., 1998, A&AS 127, 581
Rutten R.G.M., Dhillon V.S., 1994, MNRAS 28, 773
Rutten R.G.M., van Paradijs J., Tinbergen J., 1992a, A&A 260, 213
Rutten R.G.M., Kuulkers E., Vogt N., van Paradijs J., 1992b, A&A 265, 195
Savonije G.J., Papaloizou J.C.B., Lin D.N.C., 1994, MNRAS 268, 13
Sawada K., Matsuda T., Hachisu I., 1986a, MNRAS 219, 75
Sawada K., Matsuda T., Hachisu I., 1986b, MNRAS 221, 679
Sawada K., Matsuda T., Inoue M., Hachisu I., 1987, MNRAS 224, 307
Šimić D., Barwig H., Bobinger A., Mantel K.H., Wolf S., 1998, A&A 329, 115
Skilling J., 1981, Workshop on Maximum Entropy Estimation and Data Analysis, University of Wyoming, Reidel, Dordrecht, Holland
Skilling J., Bryan R.K., 1984, MNRAS 211, 111
Spruit H., 1989, In: Meyer F., Duschl W., Frank J., Meyer–Hofmeister E. (eds.) Theory of Accretion Disks. Kluwer, Dordrecht, p. 325
Spruit H., Rutten R.G.M., 1998, MNRAS 299, 768
Steeghs D., Stehle R., 1999, MNRAS 307, 99
Steeghs D., Harlaftis E.T., Horne K., 1997, MNRAS 290, L28, and 1998, Erratum, MNRAS 296, 463
Wolf S., Barwig H., Bobinger A., Mantel K.H., Šimić D., 1998, A&A 332, 984
Yukawa H., Boffin H.M.J., Matsuda T, 1997, MNRAS 292, 321

[5] But there is a prize to pay: the initial advantage of genetic algorithms usually NOT to end in side–extrema is reduced. Due to the faster convergence the population has less time to explore the parameter space with the required thoroughness.